DESIGN AND EXPERIMENTAL STUDY OF FURROW OPENER FOR SELF-PROPELLED CODONOPSIS PILOSULA TRANSPLANTER BASED ON DISCRETE ELEMENT METHOD
/
基于离散元的自走式党参移栽机开沟器设计与试验研究

Qingxu YU[1,2,3], Ying LANG[1)], Yan GONG[1)] *, Xiao ZHANG[1)], Jianling HU[1)], Dehuan ZHOU[1)],
[1)] Nanjing Institute of agricultural mechanization, Ministry of agriculture and rural areas, Nanjing, China;
[2)] Key Laboratory of Modern Agricultural Equipment, Ministry of Agriculture and Rural Affairs, Nanjing, China;
[3)] Institute of Western Agriculture, Chinese Academy of Agricultural Science, Changji, China
E-mail: yqx5205@163.com;
** Correspondent authors: Yan Gong*
DOI: https://doi.org/10.35633/inmateh-79-59

Keywords: *Codonopsis pilosula transplantation; resistance reducing furrow opener; soil transport characteristics; discrete element simulation; optimal parameter combination*

ABSTRACT
Furrow opening is a critical operation in the transplantation of Codonopsis pilosula using the seedlings-with-exposed-heads-and-film-covered-bodies (HEBCF) method. The considerable resistance generated during furrow opening results in high power consumption, making resistance reduction an important research objective. Although furrow openers have been widely studied, this study focused on the furrow opener of a self-propelled HEBCF transplanter for C. pilosula. The interaction mechanism between the furrow opener and the soil was investigated through force analysis and the development of models describing soil transport patterns and particle velocities. A discrete element simulation model of the furrow-opening process was established using EDEM to evaluate the effects of the main structural parameters on furrow-opening resistance. A three-factor five-level Box–Behnken response surface experiment was conducted, and regression models for furrow-opening resistance and soil-particle velocity were developed based on the simulation results. The structural parameters were then optimized. The optimal parameter combination consisted of a chisel-tip angle of 65°, a clearance angle of 10°, and an oblique angle of 90°. Under these conditions, furrow-opening resistance was reduced by 30.82%, while the agronomic requirements of a furrow depth of 10 cm and a furrow width of 50 cm were satisfied. These results provide a technical basis for the development and optimization of self-propelled HEBCF transplanters for C. pilosula.

摘要
开种植沟作业为党参露头覆膜移栽流程的关键环节，移栽机在执行开沟作业时会产生较大阻力，进而消耗大量动力，因此减阻开沟技术成为当前研究的首要方向。国内外研究机构针对开沟装置开展了较多研究，本文针对自走式党参露头覆膜移栽机的开沟装置，研究开沟装置与土壤的互作机理，对开沟器进行受力分析，研究土壤运移规律和速度模型；借助 EDEM 软件构建开沟仿真试验模型，全面研究相关因素对开沟阻力的影响，采用 Box-Behnken 响应曲面法设计三因素五水平的仿真试验，通过开沟性能仿真试验研究，得到开沟阻力模型和土壤颗粒速度模型，进行结构参数优化，最终确定开沟器的铲尖角 65°、隙角 10°和斜切角 90°的最优参数组合，开沟作业阻力降低 30.82%，同时满足党参移栽的开沟深度 10cm、开沟宽度 50cm 的农艺要求，为自走式党参露头覆膜移栽机研发提供支撑。

INTRODUCTION
In recent years, the market for traditional Chinese medicinal herbs has maintained a growth trend, presenting both new challenges and opportunities for the development of the related planting industry *(Wang et al., 2023)*. *Codonopsis pilosula* is one of the major traditional Chinese medicinal herbs in China, known for its effects in tonifying the middle energizer, strengthening qi, invigorating the spleen, and benefiting the lungs, earning it the reputation of "small ginseng" *(Xie et al., 2020; He et al., 2021)*.

[1] *Qingxu YU, Ph. D. Assistant Researcher; Ying Lang, Master Candidate; Yan GONG, Researcher.; Xiao Zhang, Assistant Researcher; Hu Jianling, intern researcher; Dehuan Zhou, Associate Researcher;*

The genuine production areas of *Codonopsis pilosula* are mainly distributed in the arid and semi-arid regions of Northwest China. The "*seedlings-with-exposed-heads-and-film-covered-bodies*" (HEBCF) transplanting technique is a high-quality, high-yield, and high-efficiency planting method in these arid areas. It facilitates later field management and mechanized harvesting, thereby promoting the development of full-scale mechanization *(Liu et al., 2023)*. Currently, the HEBCF transplanting process for *Codonopsis pilosula* faces the problem of a "lack of available machinery" and relies entirely on manual transplantation, which is labor-intensive, time-consuming, and incurs high costs for auxiliary workers. With the rapid development of the *Codonopsis pilosula* planting industry, the demand for specialized HEBCF transplanting machines has become increasingly urgent *(Yu et al., 2025)*. Furrow opening is the first step in the *Codonopsis pilosula* transplantation process. The considerable resistance generated during furrow opening results in high power consumption; therefore, reducing furrow-opening resistance is a major research objective. The furrow opener, one of the core components of the transplanting machine, must ensure uniform furrow depth, a neat furrow shape, and minimal soil disturbance. Its performance directly affects seedling placement posture, transplanting uniformity, and plant growth, thereby influencing the yield and quality of the crops *(Chen et al., 1961)*. Currently, there are various types of furrow openers, which can be divided into two major categories: rolling and mobile types *(Li et al., 2020)*. The rolling type includes double-disc, single-disc, axial-rotating, vertical-rotating, and chain types, while the mobile type includes core-spade, sliding knife, and boat types.

Extensive research on furrow-opening devices has been conducted both domestically and internationally, focusing primarily on the resistance reduction design of furrow-opening components, soil-component interactions, and the effects of the physical and mechanical properties of soil on furrow-opening performance *(Aikins et al., 2023)*. The forces exerted by soil on furrow openers mainly include reaction force and frictional force, which are influenced by soil shear strength, cohesion, and internal and external friction angles. Additionally, soil adhesion increases operational resistance and energy consumption. Due to the complexity of soil composition and structural heterogeneity, existing theoretical models are limited and associated calculations remain cumbersome *(Gill et al., 1983)*. To optimize the design of furrow opening components and reduce operational resistance, researchers have employed bionic design, simulation models, and field experiments to investigate the effects of structural and working parameters on soil displacement distance and traction resistance, ultimately optimizing furrow opener design *(Liu et al., 2021; Shmulevich et al., 2007; Wang et al., 2024)*. Domestic scholars have conducted extensive research on furrow openers for medicinal herb transplanters. *Wang et al., (2023),* designed a furrow opener suitable for transplanting Panax notoginseng seedlings based on the agronomic parameters of under-forest cultivation, and performed simulation analysis and experimental validation. *Chen et al., (2023),* designed a moldboard furrow opener suitable for transplanting Astragalus membranaceus. This type of furrow opener features a simple structure, ease of manufacture, and good soil penetration performance. A simulation experiment was conducted using the radius of curvature of the ridge line, the oblique angle, and the clearance angle as experimental factors, with furrow opening resistance and the coefficient of variation of furrow width as evaluation indicators. *Wang et al., (2021),* designed a sharp-angled long-wing furrow opener based on the planting pattern of long-rooted medicinal herbs in the arid regions of Northwest China, aiming to address issues such as soil accumulation and seedling exposure observed in existing medicinal herb transplanters. They simulated the operation process of the furrow opener using EDEM software, and the results demonstrated satisfactory soil covering and backfilling effects. Field experiments indicated that the performance indicators of the furrow opener met the requirements of agricultural industry standards.

Furrow opening is a critical step in the transplanting process of *Codonopsis pilosula*. During operation, the transplanting machine generates substantial resistance, leading to high power consumption. Consequently, resistance reduction technology for furrow opening has become a key research focus. Numerous research institutions worldwide have conducted extensive studies on furrow openers, and domestic scholars have also carried out relevant research on furrow openers for medicinal herb transplanters *(Feng et al., 2025; Wang et al., 2017)*. Research on furrow opening resistance reduction primarily focuses on the resistance reduction design of furrow opening components, the interaction between soil and components, and the influence of soil physical and mechanical properties on furrow opening performance—including reaction forces and friction exerted by soil on the furrow opener, soil shear strength, cohesion, and internal and external friction angles. Additionally, soil adhesion increases operational resistance and power consumption.

Due to the complex composition and structural heterogeneity of soil, existing theoretical models have limitations, and the associated calculations remain relatively complex *(Yu et al., 2009; Pan et al., 2015; Zhang et al., 2024)*. This paper focuses on the furrow opener of a Codonopsis pilosula HEBCF transplanter. It investigates the interaction mechanism between the furrow opener and the soil, analyzes the forces acting on the furrow opener, and examines soil transport patterns and velocity models. Using EDEM software, a simulation test model for furrow opening was developed to comprehensively study the effects of relevant factors on furrow opening resistance. The Box-Behnken response surface method was employed to design a three-factor, five-level simulation experiment. Through the furrow opening performance simulation, a furrow opening resistance model and a soil particle velocity model were obtained, and the structural parameters were optimized. Finally, the optimal combination of chisel tip angle, clearance angle, and oblique angle for the furrow opener was determined.

MATERIALS AND METHODS

Structural design of the furrow opener

Based on the agronomic requirements for HEBCF transplanting of *Codonopsis pilosula*, and considering the topographic characteristics of hilly and mountainous regions in Northwest China as well as the properties of cultivated soils, this study presents the design of a self-propelled HEBCF *Codonopsis pilosula* transplanter. To facilitate turning and maneuverability during transplanting operations, as well as transport and transfer, a diesel powered tracked chassis was selected as the power platform. The machine is equipped with a furrow opener, a directional transplanting device, and a soil covering and film mulching device. It is capable of performing integrated operations, including furrow opening for planting, HEBCF transplanting of *Codonopsis pilosula* seedlings, soil covering, film mulching, and edge covering. The overall structure of the transplanter is schematically shown in Figure 1.

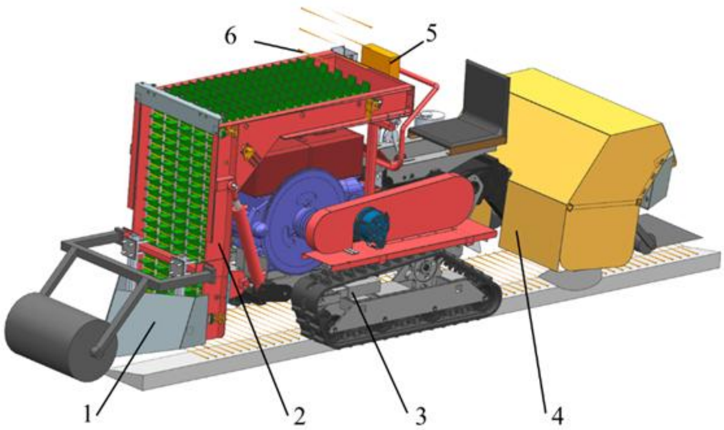

Fig. 1 - Schematic diagram of the overall structure of a transplanter

1. Ditching device, 2. Transplanting device, 3. Tracks chassis; 4. Soil covering and film covering device, 5. Transplanting electronic control system, 6. Codonopsis seedlings

The furrow opener is a key component of the HEBCF *Codonopsis pilosula* transplanting equipment. It is required to form a "V"-shaped planting furrow with a depth of 10–15 cm and a width of approximately 50 cm, with seedlings uniformly placed on one side slope of the furrow. Consistent planting depth and furrow configuration further enhance the survival rate, quality, and yield of *Codonopsis pilosula*. The furrow opener primarily consists of a furrow opener and a support wheel for furrow depth adjustment, as illustrated in Fig. 2.

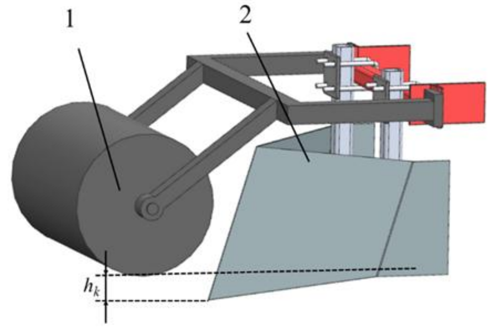

Fig. 2 - Schematic diagram of trenching unit

1. Front support wheel; 2. Furrowing device

By adjusting the mounting height of the furrow opener connecting rod, the relative height between the front support wheel and the furrow opener can be varied, thereby enabling adjustment of the furrow depth h_k. The support wheel ensures uniform furrow depth throughout the operation.

Key structural parameters of the furrow opener

Designed to satisfy agronomic requirements, the furrow opener is shown in Figure 3. Its key structural parameters are opener width (W_k), length(L_k), height (H_k), chisel tip angle (γ), clearance angle (β), and oblique cutting angle (ε). Soil on both sides backflows during trenching, so the opener width must exceed the target furrow width of 50 cm, and (W_k) is set as 52 cm in this study. The dimensions and profile of the opener depend mainly on γ, β and ε, which also affect trenching resistance and furrow cross-section shape. The chisel tip angle γ ranges 45°–75°, penetration clearance angle β is generally below 15°, and oblique cutting angle ε varies 60°–120°.

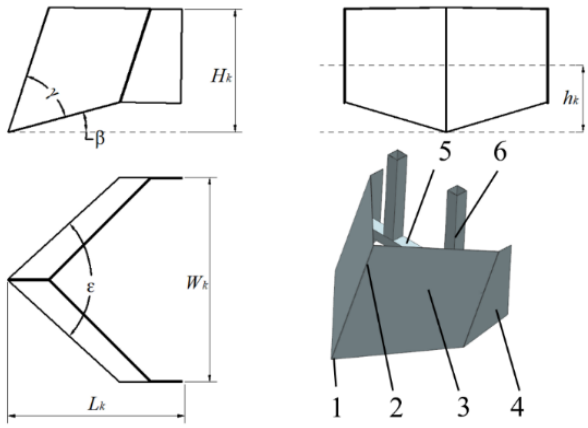

Fig. 3 - Structural diagram of a trenching opener

1. Chisel tip; 2. Cutting edge; 3. Furrow plate; 4. Side plate; 5. Supporting beam; 6. Connecting rod;

Soil characteristics of the main Codonopsis pilosula production area

Soil physical properties are a key indicator for mechanical operations and directly influence furrow opening resistance and furrow quality. In this study, soil samples were collected from the *Codonopsis pilosula* genuine producing area in Weiyuan County, Gansu Province. The soil type is sandy loam. Soil compactness was measured using a TYD-2 soil hardness tester, yielding an average value of 231.5 kPa. Measurements were also conducted in cultivated transplanting plots designated for HEBCF transplantation. The transplanting test plots were divided into six sampling areas, with random equal-volume sampling performed in each area. Surface soil samples from a depth of 0–20 cm were collected for testing, and the average moisture content of the soil samples was 16.32%. The soil samples were sieved using a standard sieve, and the proportion of particles larger than 10 mm exceeded 67.6%.

Force analysis of the furrow opener

During operation, the total force F_{Nk} acting on the furrow opener can be decomposed into the lateral force F_X along the X-axis, the forward resistance F_Y along the Y-axis, and the vertical downward force F_Z along the Z-axis. Due to the symmetrical structure of the furrow opener, the lateral forces on the left and right sides along the X-axis cancel each other out. The vertical force along the Z-axis creates a tendency for the furrow opener to penetrate the soil automatically. The power consumption of the furrow opener is primarily influenced by the force along the Y-axis. A schematic diagram of the forces acting on the furrow opener is shown in Fig.4.

During the furrow opening process, a cutting force F_T is generated at the cutting edge. After the soil undergoes shear failure, it slides backward along the furrow opener plate. The soil then exerts a normal load force F_N, tangential adhesion resistance F_S, and sliding friction force F_f on the two side plates. Subsequently, the displaced soil disperses to both sides of the furrow opener under its own gravity, resulting in relative sliding between the soil and the side plates, thereby generating a sliding friction resistance F_{Cf} on the side plates. Additionally, as the furrow opener advances, relative sliding also occurs between its bottom and the ground, causing the ground to exert a sliding friction force F_{Df} on the bottom of the furrow opener.

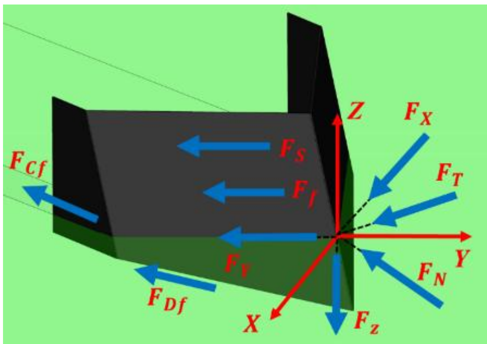

Fig. 4 - Schematic diagram of interaction between furrow opener and soil

Based on the force diagram of the furrow opener shown in Figure 5, the resistance model of the furrow opener can be derived as:

$$\begin{cases} F_X=0 \\ F_Y=F_T \sin(\gamma+\beta)+2F_N \sin(\gamma+\beta) \sin\left(\varepsilon/2\right)+2\left(F_s+F_f\right)\cos\left(\varepsilon/2\right)+2F_{Cf}+F_{Df} \\ F_Z=F_T \cos(\gamma+\beta)+2F_N \cos(\gamma+\beta)+G_k \end{cases} \tag{1}$$

where: G_k — Gravitational force of the furrow opener, N.

The normal load force F_N acting furrow opener plate is expressed as:

$$F_N=K_d S_{XZ} \tag{2}$$

where:

K_d — Resistance coefficient (N/cm²), the value of which is closely related to factors such as the structural parameters of the furrow opener plate, furrow depth, forward speed, self-weight of the furrow opener, and soil properties.

S_{XZ} — Normal cross-sectional area of soil cutting, cm².

The tangential adhesion resistance F_S on the furrow opener plate is given by:

$$F_s=N_n\mu_n+\tau_n \tag{3}$$

where:

N_n — Normal adhesion force on the furrow opener plate, N;

μ_n — Adhesion coefficient, which depends on soil properties and other factors;

τ_n — Tangential adhesion force on the furrow opener plate, N.

The friction force F_f on the furrow opener plate is expressed as:

$$F_f=F_N\mu_m \tag{4}$$

where:

μ_m — Sliding friction coefficient of the furrow opener plate, which depends on soil properties and other factors.

The friction force F_{Cf} on the side plates is given by:

$$F_{Cf}=2S_{YZ}\left(C_a+\frac{1}{2}K_0\rho_t d \tan\varphi+K_0 q \tan\varphi\right) \tag{5}$$

where:

S_{YZ} — Tangential cross-sectional area of soil cutting, cm²;

K_0 — Static earth pressure coefficient, related to soil properties and other factors;

C_a — Soil cohesion coefficient, related to soil properties and other factors;

q — Additional soil load, N;

φ — Soil internal friction angle, °;

ρ_t — Soil density, kg/m³.

The friction force F_{Df} on the bottom surface of the furrow opener is expressed as:

$$F_{Df}=F_Z \cos\beta \mu_m \tag{6}$$

Combining Equations (1) through (6), the furrow opening resistance model can be obtained as:

$$\begin{cases} F_X=0 \\ F_Y=F_T \sin(\gamma+\beta)+2K_d S_{XZ} \sin(\gamma+\beta) \sin(\varepsilon/2)+2\left(N_n\mu_n+\tau_n+F_N\mu_m\right)\cos(\varepsilon/2)+ \\ \&2S_{YZ}\left(C_a+\frac{1}{2}K_0\rho_t d \tan\varphi+K_0 q \tan\varphi\right)+F_Z \cos\beta \mu_m \\ F_Z=F_T \cos(\gamma+\beta)+2K_d S_{XZ} \cos(\gamma+\beta)+G_k \end{cases} \tag{7}$$

Analysis of soil particle dynamics

During the HEBCF transplanting operation of *Codonopsis pilosula*, the side plates must prevent premature soil backfilling into the planting furrow, thereby preserving the furrow cross-sectional shape and bottom flatness, and creating a stable and effective space for seedling placement. After the seedlings are deposited, appropriate soil backfilling helps secure the seedling tops to maintain their posture and minimize soil disturbance. Therefore, the length of the furrow opener side plates must be rationally designed, as it significantly influences both the furrow opening quality and the overall effectiveness of subsequent *Codonopsis pilosula* planting. An excessively long side plate increases furrow opening resistance, whereas an insufficiently long side plate leads to premature soil backfilling, resulting in suboptimal planting depth, furrow width, and bottom flatness, thereby compromising furrow opening quality. To further investigate the relevant parameters of the furrow opener side plates, a detailed analysis of soil particle motion characteristics on the furrow opener surface was conducted. Soil particles were assumed to be rigid granular materials that neither deform nor adhere. A specific point on the contact interface between the soil particles and the furrow opener was selected for analysis. A schematic diagram of the forces acting on the soil particles is shown in Figure 5.

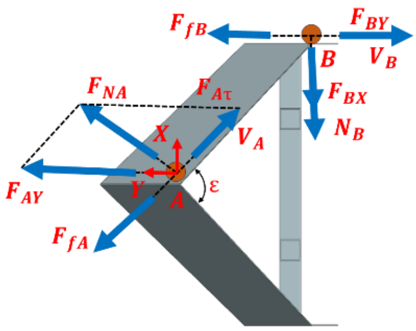

Fig. 5 - Schematic diagram of forces acting on soil particles

Assuming the soil particle is located at point A, it is subjected to a reaction force F_{NA} from the furrow opener plate and a friction force F_{fA}. The reaction force F_{NA} is first decomposed into a component F_{AY} in the forward direction (Y-axis) and a tangential component F_{At} along the furrow opener plate. The force analysis of the particle at point A yields the following equation:

$$\begin{cases} F_{AY}=\dfrac{F_{NA}}{\sin(\varepsilon/2)} \\ F_{A\tau}=\dfrac{F_{NA}}{\tan(\varepsilon/2)} \\ F_{fA}=F_{NA}\mu_m \\ F_{NA}=M_t g \cos(\gamma+\beta) \end{cases} \tag{8}$$

where:

M_t——mass of soil particles, kg;

g——gravitational acceleration, m/s².

Assuming the initial velocity of the soil particle is zero, if the tangential component $F_{A\tau}$ of the force acting on the soil particle at point A exceeds the friction force F_{fA}, the soil particle will slide at point A on the furrow opener plate. Its equation of motion can be expressed as:

$$M_t a_A = F_{A\tau} - F_{fA} \tag{9}$$

where:

a_A——acceleration of the soil particles, m/s².

Combining and rearranging Equations (8) and (9) yields:

$$M_t a_A = M_t g\cos(\gamma+\beta)\left(\frac{1}{\tan(\varepsilon/2)} - \mu_m\right) \tag{10}$$

Given that the distance from point A to point B is L_{AB}, the acceleration a_A and velocity V_A of the soil particles during its motion from point A to point B are given by:

$$\begin{cases} a_A = g\cos(\gamma+\beta)\left(\frac{1}{\tan(\varepsilon/2)} - \mu_m\right) \\ V_A = \sqrt{2g\cos(\gamma+\beta)\left(\frac{1}{\tan(\varepsilon/2)} - \mu_m\right)L_{AB}} \end{cases} \tag{11}$$

Soil particles initiate movement from point A and accelerate from rest until they reach point B at the edge of the furrow opener. Subsequently, they collide with the soil at the planting furrow edge, rebound, and continue to move along the side plate. Assuming no energy loss during this process, the interaction between the soil at the furrow edge and the moving soil particles is analyzed. The reaction force exerted by the furrow edge soil on the moving particles can be decomposed into two components in the coordinate system: the force along the X-direction, F_{BX}, and the force along the Y-direction, F_{BY}. In addition, the unmoved soil particles on both sides, characterized by the repose angle α_t, exert a normal load N_B on the moving soil particles, and the side plate exerts a friction force F_{fB} on the particles. As shown in Figure 6, based on the force analysis of the soil particles at point B, the following mechanical model can be derived:

$$\begin{cases} F_{BX} = M_t a_A \sin(\varepsilon/2) \\ F_{BY} = M_t a_A \cos(\varepsilon/2) \\ N_B = M_t g\tan\alpha_t \\ F_{fB} = (N_B + F_{BX})\mu_m \end{cases} \tag{12}$$

The differential equation of motion for the soil particle at point B along the Y-direction is:

$$M\frac{d^2y}{dt^2} = F_{BY} - F_{fB} \tag{13}$$

Combining and rearranging Equations (12) and (13) yields:

$$M_t\frac{d^2y}{dt^2} = M_t a_A\cos(\varepsilon/2) - \left(M_t g\tan\alpha_t + M_t a_A\sin(\varepsilon/2)\right)\mu_m \tag{14}$$

During the soil particle migration process, it is assumed that after moving from point A to point B, the soil particles begin to move along the side plate. Given that the length of the side plate is S, the instantaneous velocity V_B of the soil particles when they detach from the side plate can be derived as:

$$V_B = \sqrt{\left(V_A\cos(\varepsilon/2)\right)^2 + 2\left[a_A\cos(\varepsilon/2) - \left(g\tan\alpha_t + a_A\sin(\varepsilon/2)\right)\mu_m\right]S} \tag{15}$$

EXPERIMENTAL STUDY ON FURROW OPENING PERFORMANCE BASED ON DISCRETE ELEMENT METHOD

Under the condition of maintaining consistent furrow width, furrow depth, and furrow cross-sectional shape, lower furrow opening resistance corresponds to reduced power consumption. The factors directly influencing the resistance of the furrow opener include the chisel tip angle γ, clearance angle β, oblique angle ε, furrow opener width W_k, and furrow opener length L_k, as well as inherent soil properties such as adhesion and density. Among these, the furrow opener width W_k and soil adhesion are considered fixed values and are therefore not treated as experimental factors in this study. The interaction among the chisel tip angle γ, clearance angle β, and oblique angle ε affects the furrow opener length L_k, which directly influences the forward resistance in the Y-direction and the vertical penetration force in the Z-direction. Additionally, it affects the volume of backfilled soil during the furrow opening process, ultimately determining the post-furrowing cross-sectional shape. Consequently, the chisel tip angle γ, clearance angle β, and oblique angle ε are identified as key parameters and are selected as the main experimental factors.

At a given working depth, the cross-sectional area of furrow opening resistance varies with changes in the chisel tip angle γ, clearance angle β, and oblique angle ε. In this study, the furrow opening resistance per unit area, denoted as P_Y, was adopted as the evaluation index and calculated using the following equation:

$$P_Y=\frac{F_Y}{S_I} \tag{16}$$

where:

F_Y — forward resistance of the ditching tool in the Y direction, N;

S_I — Cross-sectional area of furrow opening resistance, m².

Simulation test model and experimental scheme for furrow opening

To further investigate the factors influencing furrow opening resistance, a simulation experiment on furrow opening performance was conducted using EDEM software. The soil bin in the simulation measured 1500 mm × 4000 mm × 300 mm. Single spheres were used to simulate soil particles, with a particle radius of 5 mm. The Material Block module was employed to rapidly generate soil particles, and the Hertz–Mindlin (no-slip) contact model was adopted. Extensive research has been conducted by various scholars on the sandy loam soil of Northwest China *(Dai et al., 2019)*. The relevant soil parameters for the simulation test are presented in Table 1. After the soil particles in the simulation soil bin had stabilized, the three-dimensional model of the furrow opener was imported into the simulation model. The furrow opening depth was set to 10 cm, the furrow width to 52 cm, and the forward speed to 0.18 km/h. The furrow opening performance simulation experiment is illustrated in Figure 6. Experimental data on the furrow opening resistance per unit area in the Y-direction (P_Y) were collected from the stable operation zone.

Table 1

Parameters used in the simulation experiments

Material	Parameter	Value
Soil	Poisson's ratio	0.3
	Shear modulus / Pa	5×10^7
	Density (kg·m^{-3})	2600
Steel plate	Poisson's ratio	0.3
	Shear modulus / Pa	7.9×10^{10}
	Density (kg·m^{-3})	7865
Soil-soil	Coefficient of restitution	0.21
	Coefficient of static friction	0.68
	Coefficient of rolling friction	0.27
Soil-steel plate	Coefficient of restitution	0.54
	Coefficient of static friction	0.31
	Coefficient of rolling friction	0.13

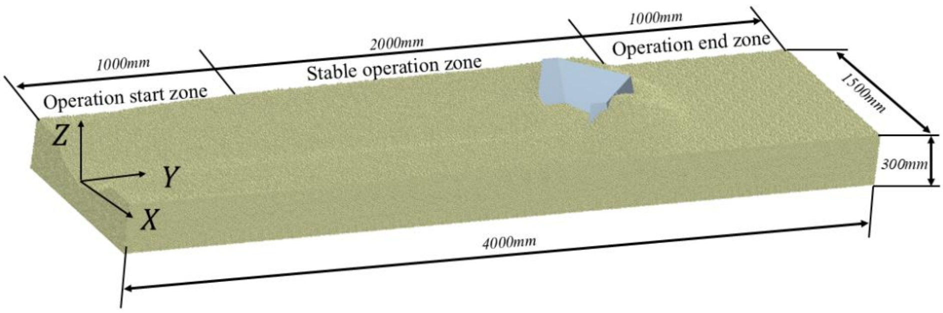

Fig. 6 - Simulation test of furrow opening performance

Through EDEM simulation experiments on furrow opening, the optimal parameter combination for the furrow opener was determined. In this study, the chisel tip angle γ, clearance angle β, and oblique angle ε were selected as experimental factors, while the furrow opening resistance per unit area in the Y-direction (P_Y) was used as evaluation indicators. A three-factor, second-order regression orthogonal rotational combination experiment was conducted to thoroughly investigate the influence of relevant factors on furrow opening performance. The coding of the simulation experiment factors is presented in Table 2, where the coded values correspond to the chisel tip angle γ, clearance angle β, and oblique angle ε, respectively. The design scheme and results of the simulation experiment are shown in Table 3, with the experimental results including the furrow opening resistance per unit area in the Y-direction (P_Y).

Table 2

Factor coding for simulation experiment

Level	Test factors		
	γ (°)	β (°)	ε (°)
1.682	75	15	120
1	69	13	108
0	60	10	90
-1	51	7	72
1.682	45	5	60

Table 3

Experimental scheme and results

Number	Test factors			Test Indicators
	γ (°)	β (°)	ε (°)	P_Y (Pa)
1	51	7	72	1685.13
2	69	7	72	1962.80
3	51	13	72	1598.33
4	69	13	72	1885.00
5	51	7	108	2161.24
6	69	7	108	2499.07
7	51	13	108	2058.64
8	69	13	108	2631.56
9	45	10	90	1772.11
10	75	10	90	2407.08
11	60	5	90	2106.61
12	60	15	90	2021.84
13	60	10	60	1632.93
14	60	10	120	2471.46
15	60	10	90	2023.67
16	60	10	90	2067.62
17	60	10	90	1945.05
18	60	10	90	2050.62
19	60	10	90	2023.67
20	60	10	90	1966.32

RESULTS AND ANALYSIS

Establishment of regression model and significance analysis

Multiple regression analysis was performed on the experimental data presented in Table 4. The regression equations relating the chisel tip angle (γ), clearance angle (β), and oblique angle (ε) to the furrow opening resistance per unit area in the Y-direction (P_Y) was obtained as follows:

$$P_Y=3643.983-52.3\gamma-152.593\beta-12.476\varepsilon+1.151\gamma\beta+0.272\gamma\varepsilon+0.458\beta\varepsilon+0.31\gamma^2 +1.773\beta^2+0.036\varepsilon^2 \tag{17}$$

Table 4 presents the significance test results for the regression equations. The p-values for both the P_Y models are less than 0.01, indicating that the goodness of fit is highly significant and that the established models are reliable. The effects of γ, ε, and their interaction γ,ε on P_Y are highly significant (p< 0.01), while the effects of other factors on P_Y are not significant.

Table 4

Analysis of variance for the regression model

Source	P_Y - Experimental Results				
	Sum of squares	Degree of freedom	Mean Square	*F*-value	*P*-value
model	1483083.5	9	164787.06	77.82	<0.0001**
γ	473514.8	1	473514.83	223.62	<0.0001**
β	5629.2	1	5629.22	2.66	0.1341
ε	964577.0	1	964576.95	455.53	<0.0001**
γ*β*	7447.7	1	7447.74	3.52	0.0902
γε	14999.0	1	14998.96	7.08	0.0238**
*β*ε	4727.9	1	4727.90	2.23	0.1660
γ^2	8753.1	1	8753.13	4.13	0.0694
β^2	3540.9	1	3540.92	1.67	0.2250
ε^2	1879.9	1	1879.87	0.89	0.3683
Residual	21174.8	10	2117.48		
Lack of fit	9752.1	5	1950.43	0.85	0.5668
Pure error	11422.6	5	2284.52		
Total	1504258.3	19			

*Note: * indicates significant effect (P<0.05), ** indicates high significant effect (P<0.01)*

The coefficients of determination (R^2) for the regression equations are 0.9859 and 0.9771, respectively, both close to 1, indicating that the deviations between the predicted values and the actual values are minimal and nearly coincident. This demonstrates that the models accurately capture the relationship between the experimental factors and the response indicators. For the furrow opening resistance per unit area in the Y-direction (P_Y), the predicted R^2 and adjusted R^2 are both 0.9332, with a difference of less than 0.2. This indicates that the model exhibits excellent explanatory and predictive capabilities, and the high consistency between the two suggests that the model is not overfitted.

Figures 7(a) present the residual versus predicted value plots for the furrow opening resistance per unit area in the Y-direction (P_Y), respectively. The residual points for P_Y are randomly distributed with no discernible systematic pattern, indicating that the model fitting does not exhibit significant bias. Additionally, the residuals do not display a funnel-shaped pattern and are randomly scattered within the range of ±3 standard deviations (indicated by the red lines), suggesting the absence of significant outliers. Furthermore, the influence of individual data points on the estimation of model parameters is controllable, which further enhances the reliability of the established models.

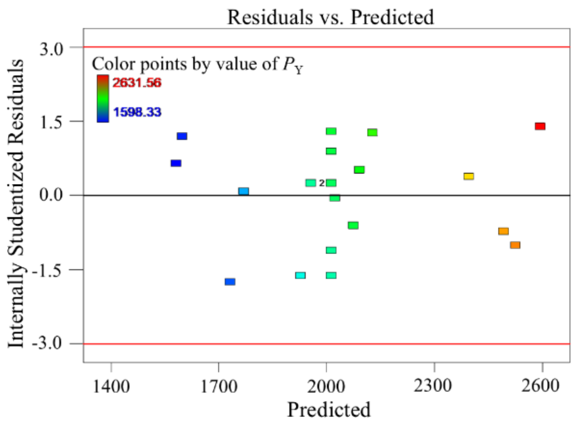

Fig. 7 - Residuals-versus-predicted plot for P_Y

Analysis of Furrowing Resistance per Unit Area in the Y-Direction (P_Y)

Box plots enable a rapid comparison of response distributions across different factor levels, facilitate the identification of outliers and data dispersion characteristics, and assist in evaluating the main effects and potential interactions of factors. To investigate the individual effects of the chisel tip angle (γ), clearance angle (β), and oblique angle (ε) on the furrow opening resistance per unit area in the Y-direction (P_Y), box plots were constructed for each factor against P_Y, as shown in Figure 8.

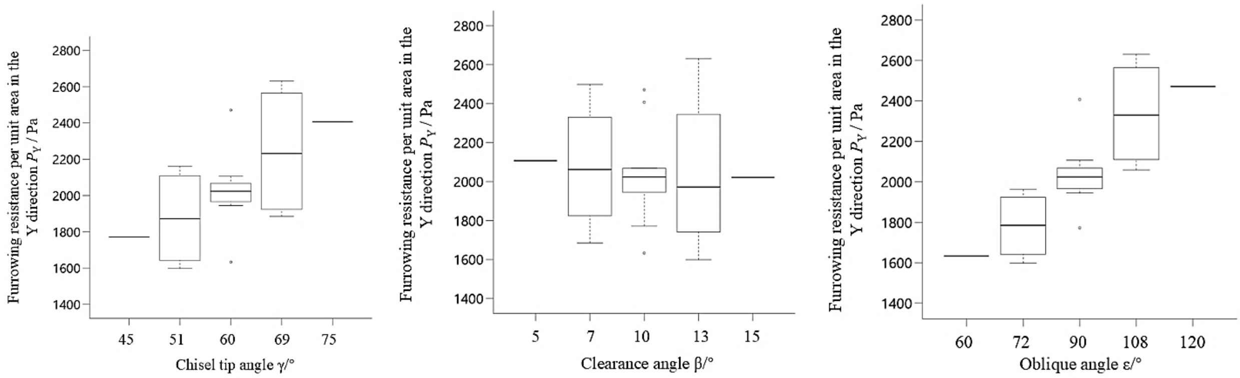

Fig. 8 - Box plot of P_Y

As shown in Figure 8(a), when the chisel tip angle (γ) is at levels −1, 0, and 1, the median values of the furrow opening resistance per unit area in the Y-direction (P_Y) are 1871.88, 2023.67, and 2230.93, respectively. P_Y exhibits a generally rapid increasing trend with increasing γ. At level 1 of γ, the box height is the largest, indicating the highest dispersion of P_Y data, which may lead to greater result variability and reduced data stability. To minimize P_Y, a low level of γ is preferable. As shown in Figure 8(b), when the clearance angle (β) is at levels −1, 0, and 1, the median values of P_Y are 2062.02, 2067.62, and 1971.82, respectively. P_Y initially shows a slight decreasing trend followed by a marginal increase as β increases. An optimal range for minimizing P_Y exists near level 1 of β. However, at level 1 of β, the box height is the largest and the whiskers are longer, indicating high dispersion of P_Y data, necessitating further collaborative optimization analysis considering other factors. As shown in Figure 8(c), when the oblique angle (ε) is at levels −1, 0, and 1, the median values of P_Y are 1785.07, 2023.67, and 2330.15, respectively. P_Y generally exhibits a rapid increasing trend with increasing ε. To minimize P_Y, a low level of ε is preferable.

To further investigate the interactive effects of the chisel tip angle (γ), clearance angle (β), and oblique angle (ε) on the furrow opening resistance per unit area in the Y-direction (P_Y), the influence of factor interactions on P_Y is illustrated in Figure 9.

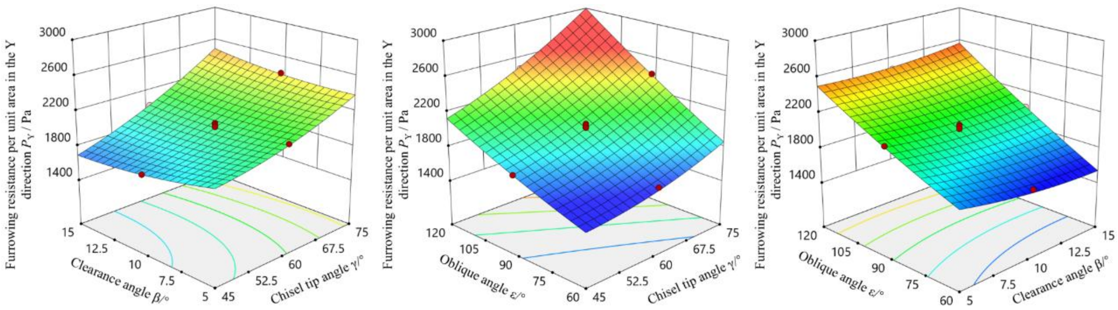

Fig. 9 - The interaction effects of various factors on P_Y

As shown in Figure 9(a), when the chisel tip angle (γ) is small, the furrow opening resistance per unit area in the Y-direction (P_Y) gradually decreases with increasing clearance angle (β); conversely, when γ is large, P_Y gradually increases with increasing β. When β is within the range of 5° to 15°, an increase in γ consistently leads to an increase in P_Y. Therefore, a combination of a smaller γ and a larger β yields a lower P_Y. As shown in Figure 9(b), when the oblique angle (ε) is within the range of 60° to 120°, an increase in γ results in an increase in P_Y. Similarly, when γ is within the range of 45° to 75°, an increase in ε also leads to an increase in P_Y. Both γ and ε exhibit a positive linear relationship with P_Y. Accordingly, a parameter combination of a smaller γ and a smaller ε yields a lower P_Y. As shown in Figure 9(c), when β is within the range of 5° to 15°, an increase in ε consistently leads to an increase in P_Y. When ε is small, P_Y gradually decreases with increasing β; when ε is large, P_Y gradually increases with increasing β. Under these conditions, a combination of a larger β and a smaller ε yields a lower P_Y.

Parameter optimization and simulation performance verification

Based on the established regression models, the influence patterns of the chisel tip angle (γ), clearance angle (β), and oblique angle (ε) on the furrow opening resistance per unit area in the Y-direction (P_Y) was obtained, facilitating an in-depth analysis of the mechanistic effects of these factors on resistance during the furrow opening process. The furrow opening resistance is closely related to γ, β, and ε. In this study, the optimization module of Design-Expert software was employed, with the optimization objectives set as minimizing P_Y, thereby ensuring low and stable furrow opening resistance. A multi-objective optimization mathematical model was established to determine the optimal parameter combination. The objective functions and constraint equations are as follows:

$$\begin{cases} min\, P_Y(\gamma,\ \beta,\ \varepsilon) \\ s.t. \begin{cases} 45 \le \gamma \le 75 \\ 5 \le \beta \le 15 \\ 60 \le \varepsilon \le 120 \end{cases} \end{cases} \tag{19}$$

Multiple sets of optimal parameter combinations were obtained. An increase in the oblique angle (ε) increases furrow opening resistance but also facilitates soil penetration. Considering manufacturability, furrow opener length, and the overall machine layout, the oblique angle ε was selected as 70°, with the optimized chisel tip angle γ = 55° and clearance angle β = 15°. The resistance-reducing furrow opener with the optimal parameter combination is shown in Figure 10. Under these conditions, the furrow opening resistance per unit area in the Y-direction (P_Y) is relatively low, and the penetration force acts in the negative Z-direction, which is conducive to soil penetration during furrow opening operations.

(a) 3D model (b) Physical object

Fig. 10 - Resistance-reducing furrow opener

To further verify the performance of the furrow opener with the optimal parameter combination in actual furrow opening operations, a simulation performance verification was conducted. The furrow opening resistance curve obtained from the simulation test is shown in Figure 11, which illustrates the variation of furrow opening resistance of the optimized furrow opener in the simulated environment, providing an important basis for further in-depth investigation of its performance characteristics. The measured furrow opening resistance in the Y-direction was 500.55 N, the furrow opening resistance per unit area in the Y-direction (P_Y) was 1587.30 Pa. Compared with the initial furrow opener (γ = 65°, β = 10°, ε = 90°), the furrow opening resistance in the Y-direction was reduced by 228.92 N, corresponding to a reduction rate of 30.82%.

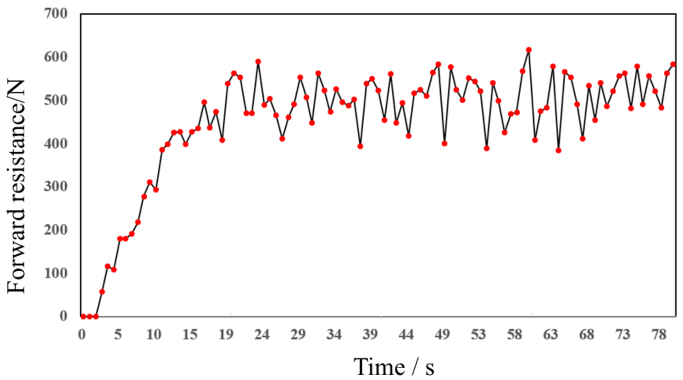

Fig. 11 - Simulation performance test trench resistance curve

Bench test verification of the furrow opener

Verification analysis of furrow opening resistance

A furrow opening resistance verification test was conducted at the research base of Gansu Agricultural University. The soil used in the test was collected from a genuine production area of *Codonopsis pilosula* in Northwest China. The soil moisture content was measured as 15.0% using an LHS16-A halogen moisture meter. Prior to the test, the soil was rotary tilled to simulate the actual transplanting environment. A furrow opener prototype with a chisel tip angle (γ) of 55°, oblique angle (ε) of 70°, clearance angle (β) of 15°, and width (W_k) of 52 cm was mounted on the traction frame of the furrow opener above the soil bin. After each test, the soil in the bin was rotary tilled again, as shown in Figure 12.

Fig. 12 - Bench test for trenching performance

As shown in Figure 13, the results obtained from the EDEM simulation were highly consistent with the actual operation of the furrow opener. The furrow profile predicted by the EDEM simulation closely matched the width, depth, and shape of the planting furrow formed during actual operation. Regarding soil flow direction, the EDEM simulation accurately reproduced the flow path and distribution of soil during the furrow opening process, demonstrating strong agreement with the actual soil flow observed under field conditions. To a considerable extent, the EDEM simulation method reflected the real working conditions of the furrow opener, providing a powerful tool for in-depth investigation of its operating principles and performance characteristics. It enabled the optimization and adjustment of structural and working parameters within a simulated environment and allowed for the prediction of furrow opener performance in advance. Consequently, this approach reduced the number and cost of physical experiments, thereby improving the efficiency and quality of the design and optimization process for the furrow opener.

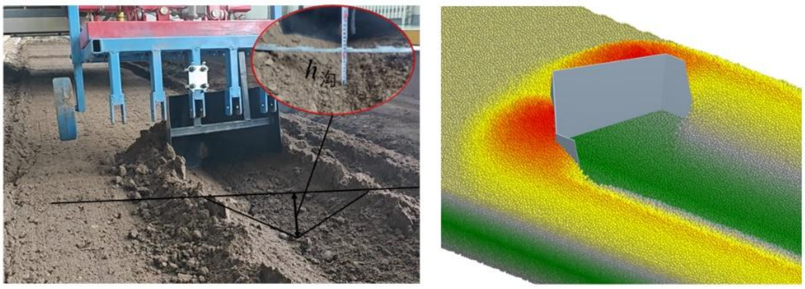

Fig. 13 - Comparative test between simulation and bench trenching operations

The test bench utilized an electric variable-frequency four-wheel-drive soil bin test vehicle as the power source, with the furrow opener attached via a three-point hitch for furrow opening operations. The test bench was equipped with an automated measurement system capable of simultaneously recording forward resistance and vertical resistance, with a data acquisition frequency set to 10 Hz. The operating parameters were consistent with those used in the simulation performance test: the furrow opening depth was set to h_k = 10 cm, the forward speed to 0.18 km/h, and each test run had a length of at least 3 m. The acquired data were processed using a moving average algorithm, and a curve of furrow opening resistance over time was plotted. The furrow opening resistance curve obtained from the bench performance test is shown in Figure 17. As shown in Figure 14, the average forward furrow opening resistance obtained from the bench test was 552.64N, with a relative error of 9.43% compared to the simulation result. Comparison between the simulated and experimental values indicates that the error in forward furrow opening resistance is relatively small, suggesting that the simulation results can reliably reflect the actual forward resistance of the furrow opener.

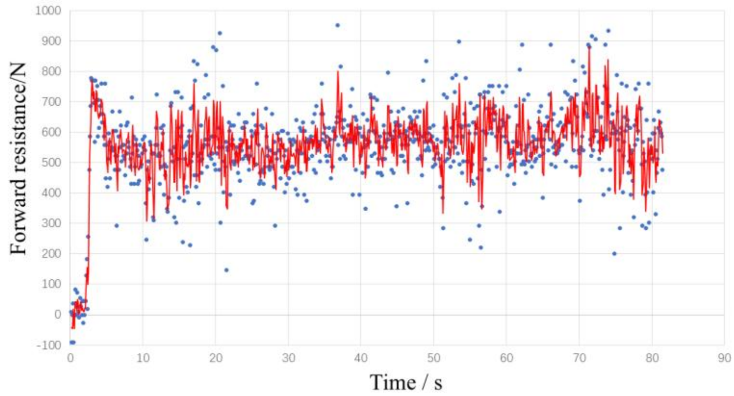

Fig. 14 - Trench resistance curve for bench performance test

CONCLUSIONS AND DISCUSSION

(1) The interaction between the furrow opener and the soil was investigated theoretically to address the high furrow-opening resistance encountered in the sandy loam soils of the main *Codonopsis pilosula* production region. The forces acting on the furrow opener and the soil during furrow opening were analyzed, and a resistance model for the furrow opener was established. The relationships among furrow-opening resistance, the intrinsic properties of the soil, the furrow cross-sectional area, and the structural parameters of the furrow opener were examined. The dynamic behavior of the soil particles during furrow opening was also investigated, and a mathematical model describing the particle velocity at detachment from the side plate was derived. This velocity was related to structural parameters such as the chisel-tip angle. The theoretical analysis indicated that, under fixed soil conditions, the chisel-tip angle, clearance angle, and oblique angle are the principal structural factors affecting furrow-opener performance.

(2) Furrow-opening performance was evaluated through discrete element simulations conducted using EDEM. A three-factor simulation experiment was designed using response surface methodology. Evaluation indicators, including furrow-opening resistance per unit area and penetration force, were defined, and a virtual soil-bin test platform was developed. Multiple regression analysis and analysis of variance were performed on the simulation results, yielding a highly significant regression model for the furrow-opening resistance per unit area in the *Y*-direction, P_Y. Residual analysis and box-plot analysis supported the adequacy and reliability of the model for optimizing the structural parameters of the furrow opener. The results showed that the chisel-tip angle was positively correlated with furrow-opening resistance. The clearance angle exhibited a positive linear relationship with penetration force but had only a limited effect on furrow-opening resistance, whereas the oblique angle significantly affected the evaluated performance indicators.

(3) Multiobjective optimization was conducted to determine the preferred structural parameter combination. An optimization model was established with the objective of minimizing the furrow-opening resistance per unit area in the *Y*-direction, P_Y. The selected optimal combination consisted of an oblique angle of 70°, a chisel-tip angle of 55°, and a clearance angle of 15°. Simulation verification showed that, after optimization, the furrow-opening resistance in the *Y*-direction was 500.55 N and P_Y was 1587.30 Pa, corresponding to a resistance reduction of 30.82%. Bench tests were subsequently conducted to validate the simulation results. The mean forward resistance measured in the bench tests was 552.64 N, resulting in a relative error of 9.43% compared with the simulated value. This level of agreement indicates that the simulation model can provide a useful basis for the structural optimization of resistance-reducing furrow openers for *C. pilosula* transplanting.

ACKNOWLEDGEMENT

We would like to thank all colleagues for their advice and support throughout the research process.

REFERENCES

[1] Aikins, K. A., Ucgul, M., Barr, J. B., Awuah, E., Antille, D. L., Jensen, T. A., Dwsbiolles, J. M. E. (2023). Review of discrete element method simulations of soil tillage and furrow opening. *Agriculture*, Vol. 13(3), Switzerland.

[2] Chen, E. (1961). Plowing Depth and the Layered Development of the Plow Layer (耕翻深度与耕层的层次发育), *Chinese Agricultural Science*, Vol. 2(12), PP. 1-6, Beijing/China.

[3] Chen, H., Qi, W., Wang, J., Zhang, J., Ma, A. (2023). Design of Moldboard Plow Openers Based on Discrete Element Method and Response Surface Method (基于离散元法和响应面法的铧式开沟器设计), *Mechanical Design*, Vol. 40(1), pp. 65-71, Tianjin/China.

[4] Dai, F., Song, X., Zhao, W., Zhang, F., Ma, A., Ma, M. (2019). Simulative Calibration on Contact Parameters of Discrete Elements for Covering Soil on Whole Plastic Film Mulching on Double Ridges (全膜双垄沟覆膜土壤离散元接触参数仿真标定), *Transactions of the Chinese Society for Agricultural Machinery*, Vol. 50(2), pp. 49-56,77, Beijing/China.

[5] Feng, B., Shi, L., Xin, S., Wang, G., Sun, W., Wang, J., Wang, S. (2025). Optimization and Experiment of Ditcher Parameters for Astragalus membranaceus Transplanter (黄芪移栽机开沟器参数优化与试验). *Journal of Agricultural Mechanization Research*, Vol. 47(10), pp. 189-196, Haerbin/Heilongjiang

[6] He, R., Jin, Z., Ma, R., Hu, F., Dai, J. Network pharmacology unveils spleen-fortifying effect of Codonopsis Radix on different gastric diseases based on theory of "same treatment for different diseases" in traditional Chinese medicine. *China Herbal Medicines*, Vol. 13(2), pp. 189-201, Tianjin/China.

[7] Li, B. (2020). Agricultural Mechanization (农业机械学). *China Agriculture Press*，Beijing/China.

[8] Liu, J., Li, Q., Zheng, X., Wang, Z. (2021). Research Status of Drag Reduction Technology for Soil Tillage Components (土壤耕作部件减阻技术研究现状). *Xinjiang Agricultural Mechanization,* pp. 25-28,37, Wulumuqi/Xinjiang.

[9] Liu, J., Zhang, J. (2023). A Brief Analysis of the Fully Mechanized Cultivation Technology of Dangshen with Mulching in Semi-Arid Mountain Areas (浅析半干旱山区党参露头覆膜全程机械化种植技术). *Agricultural Machinery*, pp. 57-59,62, Haerbin/Heilongjiang.

[10] Pan, S. (2015). Research on the Optimization Design and the Experiment of the Core Ploughshare Furrow Opener Based on the Discrete Element Method (基于离散元法的芯铧式开沟器优化设计与试验研究). *Jilin University,* Changchun/Jilin.

[11] Shmulevich, I., Asaf, Z. (2007). Rubinstein D. Interaction between soil and a wide cutting blade using the discrete element method. *Soil & Tillage Research*, Vol. 97(1), pp. 37-50, Netherland.

[12] Wang, F., Chen, S., Liu, Y., Chen, H., Hu, Y., Li, S., Chen, L. (2023). Advances and Prospects of Chinese Herbal Medicine Planting Industry in China (我国中药材种植产业进展与展望). *Mod Chin Med*, Vol. 25(6), pp. 1163-1171, Beijing/China.

[13] Wang, J. (2023). Optimized design and research of trenching components for panax notoginseng transplanting (三七移栽开沟部件的优化设计与研究). *Kunming: Yunnan Agricultural University*, Kunming/Yunnan.

[14] Wang, J., Sun, W., Wang, H., Zhang, H., Liu, X. (2021). Research of Long Wing and Sharp Angle Opener (尖角长翼型开沟器的研究). *Agricultural Mechanization Research*, Vol. 43(11), pp. 64-70, Haerbin/Heilongjiang.

[15] Wang, L., Zhou, B., Wan, C., Zhou, L. (2024). Structural parameter optimization of a furrow opener based on EDEM software. *International Journal of Agricultural & Biological Engineering*, Vol. 17(3), pp. 115-120, Beijing/China.

[16] Wang, X. (2017). Design and experimental study of key components for inclined licorice transplanting (甘草倾斜移栽关键部件设计与试验研究). *China Agricultural University*, Beijing/China.

[17] W. R. Gill., G,.E, VandenBerg. (1983). Tillage and Traction Soil Dynamics (耕作和牵引土壤动力学). *China Agricultural Machinery Press*, Beijing/China.

[18] Xie, Q., Sun, Y., Cao, L., Chen, L., Chen, J., Cheng, X., Wang, C. (2020). Antifatigue and antihypoxia activities of oligosaccharides and polysaccharides from *Codonopsis pilosula* in mice. *Food Funct*, Vol. 11(7), pp. 6352-6362, United Kingdom.

[19] Yu, J., Qian, L., Yu, W., Pan, S., Fang, Y., Fu, H. (2009). Analysis of the Resistances Applied on Furrow Openers (开沟器工作阻力的离散元法仿真分析). *Transactions of the Chinese Society for Agricultural Machinery*, Vol. 40(06), pp. 53-57, Beijing/China.

[20] Yu, Q., Li, R., Gong, Y., Ma, Y., Chen, X., Hu, J. (2025). Research status and development trends of mechanized transplanting of *Codonopsis pilosula* (党参移栽机械化研究现状与发展趋势). *Journal of Chinese Agricultural Mechanization*, Vol. 46(05), pp. 34-42, Nanjing/Jiangsu.

[21] Zhang, B., Yang, X., Zhu, Y. (2024). Design and Simulation of a Combined Trencher for Transverse Sugarcane Planter. *Agriculture*, Vol. 14(8), pp. 1416-1416, Netherland.